RASĀYAN *J. Chem.*
Vol. 19 | No. 2 | 1209-1216 | April-June | 2026
ISSN: 0974-1496 | e-ISSN: 0976-0083 | CODEN: RJCABP
http://www.rasayanjournal.com
http://www.rasayanjournal.co.in

SYNTHESIS AND CHARACTERIZATION OF $CaCO_3$-TIO_2 NANOCOMPOSITES FOR POTENTIAL NANOLUBRICANT APPLICATIONS

M. Deekshitha, Y.V.V.S.N. Murthy✉, J. Narayanan, and Sandeep Kumar
School of Marine Engineering and Technology, Indian Maritime University,
Chennai-600119, (Tamil Nadu) India
✉Corresponding author: yvvsnmurthy@imu.ac.in

ABSTRACT

Calcium carbonate ($CaCO_3$)-modified titanium dioxide (TiO_2) nanoparticles (NPs) were synthesised by a combined sol-gel and wet impregnation method to achieve controlled surface and structural modifications for multifunctional applications. The incorporation of $CaCO_3$, an environmentally compatible dopant, into the TiO_2 matrix was carried out to build physicochemical properties while maintaining high surface reactivity. XRD analysis confirmed the predominance of the anatase phase, with slight variations in peak, suggesting the influence of $CaCO_3$ incorporation. Synthesised sample indicating the formation of well-defined nano-flower structures, while elemental analysis indicates uniform dopant distribution within the TiO_2 framework. These particles exhibited increased crystallinity and a controlled particle-size distribution, indicating moderate dispersion stability with limited aggregation. These structural and surface modifications are indicative of characteristics desirable for nano-lubricant applications, particularly for friction reduction, wear resistance, load-bearing performance, surface interaction and stability. Furthermore, the modified material suggests its suitability as a multifunctional candidate for sustainable industrial applications. Overall, this study highlights the role of $CaCO_3$ doping in tuning TiO_2 properties and provides a base for future experimental studies in tribological and environmental domains.

Keywords: TiO_2 Nanoparticles; $CaCO_3$ Doping; Sol–Gel Synthesis; Wet Impregnation; Nanocomposites; Dispersion Stability; Nano-Lubricants.

RASĀYAN *J. Chem.*, Vol. 19, No. 2, 2026

INTRODUCTION

Friction and wear in mechanical systems lead to significant energy losses and reduced efficiency in industrial applications. In recent years, the development of advanced nanomaterials has attracted attention towards these challenges. In the field of nanoscale lubrication systems, Titanium oxide nanoparticles (NPs) exhibit properties like huge surface area, photocatalytic activity and reaction stability. These properties make titanium dioxide(TiO_2) an attractive additive for various industrial applications, including catalysis, coatings, environmental remediation and lubrication.[1-3] These NPs establish several flexible approaches, including sol-gel, electrochemical anodization, green synthesis (biological), chemical vapour deposition, solvothermal, microwave-assisted synthesis, and hydrothermal methods.[4-7] In this study, the synthesis process focuses on developing nanostructured materials with characteristics relevant to lubrication-related applications and environmental considerations. The sol-gel method involves hydrolysis followed by condensation reactions, enabling controlled particle formation.[8,9] This process introduces n-hexane, a nonpolar solvent, which helps in controlling the rate of reaction and particle size.[10] Having a high surface area of TiO_2 NPs, adsorption of molecules onto the surface is enhanced, which can influence reaction kinetics by increasing molecular interactions.[11] Further functional properties were improved by the doping process with suitable materials, where an effective strategy has been explored for modifying the electronic structure and surface characteristics.[12] In this context, calcium carbonate ($CaCO_3$) was introduced as a dopant, which was a naturally abundant, environmentally benign and cost-effective material widely used as an additive in polymers, paints, and lubricants.[13] The TiO_2 particles were doped by $CaCO_3$ through the wet-impregnation method, where these nanostructures are dispersed and incorporated into the $CaCO_3$ matrix. This process of hybridisation develops the dispersion stability of TiO_2 and reduces agglomeration. The formation of TiO_2-$CaCO_3$ composite suggests the thermal stability

http://doi.org/10.31788/RJC.2026.1929653

and load-bearing capacity, which are majorly focused on in tribological applications.[13-15] Previous studies have reported that TiO_2-based nanomaterials can contribute to friction reduction and wear resistance when used as lubricant additives. In such systems, TiO_2 may act as rolling elements at contact interfaces, while $CaCO_3$ can assist in surface smoothing and tribofilm formation.[14,16] These kinds of mechanisms are associated with improved load-carrying capacity and reduced surface damage. Such nano-additives are considered eco-friendly and align with sustainability goals, particularly in improving energy efficiency in industrial systems. The $CaCO_3$-doped TiO_2 nanocomposite is expected to enhance the durability and service life of mechanical components in the lubrication system.[14,15] However, despite extensive studies on TiO_2 NPs, limited studies have reported on $CaCO_3$-modified TiO_2 synthesised via wet-impregnation, particularly in the context of nano-lubricant applications. This highlights the need for systematic investigation of such hybrid nanostructures[12,13]. Therefore, the present work is on the synthesis of $CaCO_3$-doped TiO_2 nanocomposite, followed by characterisation, detailing the structural and morphological aspects. Although tribological performance was not experimentally evaluated, the obtained results provide insights into their potential applicability in nano-lubricant systems.

EXPERIMENTAL

Materials and Methods

Titanium tetrachloride ($TiCl_4$, 99.5%), n-hexane (95%), calcium carbonate ($CaCO_3$, 99.5%), ethanol (99%), deionized water (pH 5.5–7.5), and hydrochloric acid (HCl, 35–37%) were used in this study. $TiCl_4$ served as the precursor for TiO_2 synthesis, n-hexane acted as a dispersing solvent, and $CaCO_3$ was used as the dopant. The synthesis process using the sol–gel method, followed by wet impregnation for doping.

General Procedure

Synthesis of TiO_2

Titanium dioxide was synthesised by a sol-gel method[8,9] with slight modifications, a well-established approach for producing oxides with proper size and phase composition. Initially, in a clean, glass beaker, 0.0912 mol of $TiCl_4$ was slowly added to a well-stirred mixture of n-Hexane and deionised water (maintained at room temperature). Due to the highly reactive nature of $TiCl_4$ with atmospheric moisture, the handling was carried out carefully, with appropriate precautions in a well-ventilated environment to minimise exposure to fumes. Then, the sample mixture was placed on a magnetic stirrer with a hot plate, maintaining the temperature at approximately 60 °C and stirring at 600 rpm to promote controlled hydrolysis and condensation reactions typical of sol-gel chemistry. While stirring, dilute HCl (0.1M) was added dropwise to peptize and stabilise the forming TiO_2 sol. A white precipitate of hydrated titanium species was formed. The suspension was further stirred for 1 h to ensure full hydrolysis and uniform dispersion. The suspension was centrifuged to separate the precipitate and then transferred into a crucible. Crystallization and phase stabilisation were achieved by calcination at 500 °C for 2 h. This thermal treatment removed residual water or organics and converted the gel into crystalline TiO_2. The final yield of TiO_2 obtained was approximately 5.0 g.

Doping of TiO_2 with $CaCO_3$

$CaCO_3$ doping was carried out by the wet-impregnation method.[12] Initially, 2 g of synthesised TiO_2 and the required amount of $CaCO_3$ were dispersed separately in 6 ml of ethanol under stirring to form uniform suspensions. The $CaCO_3$ suspension was then gradually mixed with the TiO_2 suspension under continuous stirring. The sample was stirred at approximately 60 °C for 1-2 h to ensure proper interaction between TiO_2 and $CaCO_3$. After completion of the mixing process, the resulting suspension was centrifuged to separate the precipitate. The obtained solid was dried and subsequently calcined at 200 °C, 2h in a muffle furnace to obtain $CaCO_3$-doped TiO_2 nanoparticles. The final product (3.0 g) was collected for further characterisation. The synthesis procedure is illustrated in Fig.-1.

RESULTS AND DISCUSSION

X-ray Diffraction (XRD)

The synthesised TiO_2 and $CaCO_3$-doped TiO_2 were examined using an XRD pattern, which was used on a PANalytical diffractometer using Cu kα radiation (λ = 1.54060 Å) at 25 °C, over a 2θ range of 5.01-

99.98° (step size 0.022°, scan step time[s] 58.3950, continuous scan; generator 15mA 40kV). with Cu Kα radiation ((λ = 1.54060 *Å*). The diffraction pattern exhibited a prominent peak at 2θ ≈ 25.2°,
Scherrer equation was given below to calculate the average crystallite size[17]:

$$D = \frac{k\lambda}{\beta \cos\theta}$$

Where k = dimensionless constant
θ = diffraction angle
λ = wavelength of the X-ray radiation
β = full width at half-maximum (FWHM) of the diffraction peak.

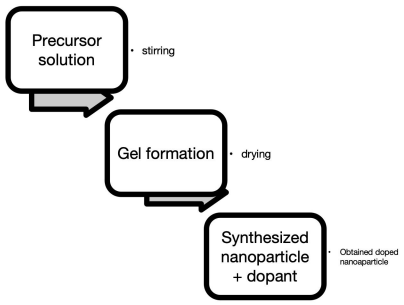

Fig.-1: A Quick Flow Chart Representing the Procedure of Synthesizing and Doping a Nanomaterial

XRD Analysis of Synthesized TiO_2

The synthesized nanostructure (Fig.-2(a)) shows a dominant diffraction peak at 2θ= 25.2183° (d= 3.53157Å), which is indexed to the (101) plane of anatase TiO_2 (JCPDS 21-1272). Other minor peaks are observed at approximately 35.99° (004), 41.15° (111), 47.94° (200), 54.22° (211) and 27.36° (110), which is also considered a secondary peak corresponding to the rutile TiO_2, indicating a minor rutile phase. The diffraction indicates mixed anatase and rutile phases, with anatase (101) at 25.21° as the dominant reflection, consistent with the reported literature.[1] Anatase (101) was estimated from the Scherrer equation, found to be in the nanometer range (≈ 15-20 nm), confirming the nanoscale formation. Impurity peaks were not observed, indicating successful synthesis of crystalline TiO_2.

XRD Analysis of $CaCO_3$-Doped TiO_2

The XRD pattern of $CaCO_3$-doped TiO_2 nanocomposite exhibited multiple diffraction peaks (Fig.-2(b)), indicating the presence of both TiO_2 and $CaCO_3$ phases. The prominent peak at 2θ ≈ 25.19° with a relative intensity of 38.81% corresponds to the (101) plane of anatase TiO_2, confirming the retention of the anatase structure after doping. The most intense peak observed at 2θ ≈ 27.31° (100% intensity) corresponds to the (110) plane of rutile TiO_2, indicating the presence of minor rutile phase along with the dominant anatase structure.

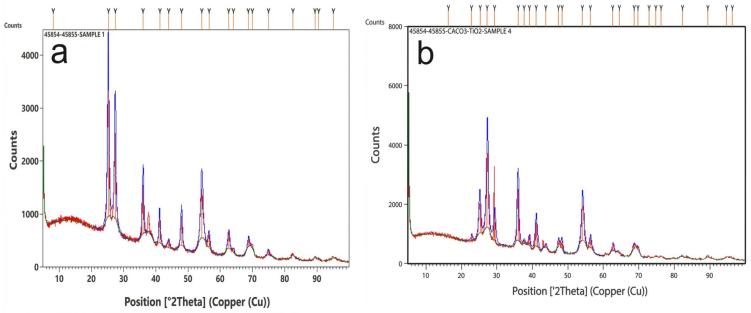

Fig.-2: TiO_2 and $CaCO_3$-doped TiO_2 by XRD Patterns are Shown in Fig.-2(a) and Fig.-2(b), respectively

Additionally, a characteristic peak at 2θ ≈ 29.38° with ~29% intensity is attributed to the (104) plane of $CaCO_3$ (calcite phase), confirming its incorporation into the TiO_2 matrix. Other diffraction peaks observed at 2θ values of 35.94°, 41.11°, 48.32°, 54.17°, and 56.39° further support the presence of a

mixed-phase nanocomposite structure. The variation in peak intensities and positions suggests structural modification due to $CaCO_3$ incorporation, while maintaining the crystalline nature of TiO_2. The crystallite-doped sample, calculated using the Scherrer equation, was found to be approximately 13-14 nm, indicating a nanocrystalline composite.

Scanning Electron Microscopy-Energy Dispersive X-ray Spectroscopy (SEM-EDS)

SEM coupled with EDS was used for TiO_2 and $CaCO_3$-doped TiO_2 samples to examine the surface morphology and elemental composition. The EDS measurements were done by accelerating voltage of 20 kV with live acquisition times of approximately 120 s and low dead-time values (1-2%). Elemental compositions were normalised to 100% after excluding Al signals originating from the sample holder.

SEM-EDS Analysis of Synthesized TiO_2

The SEM micrographs of TiO_2 (Fig.-3(a)) show agglomerated NPs forming a hierarchical nanostructure with a relatively rough surface. The primary particle size is in the nanometer range, with larger clusters resulting from agglomeration. The EDS spectrum (Fig.-4(a)) of the synthesized TiO_2 sample confirms Ti and O presence as the major elements. The normalised mass concentrations were 55.15 wt% Ti and 44.85 wt% O, corresponding to atomic concentrations of 29.12 wt% Ti and 70.88 wt% O. The Ti:O atomic ratio is close to the expected 1:2 stoichiometry of TiO_2, indicating successful formation of the oxide phase. No additional impurity peaks were detected. The corresponding EDS elemental mapping (Fig.-4b) shows a uniform spatial distribution of Ti and O throughout the sample, confirming compositional homogeneity.

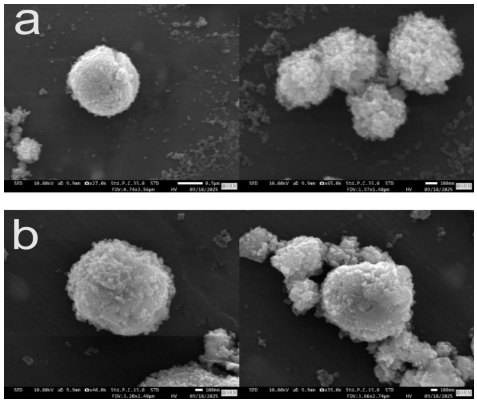

Fig.-3: SEM Micrographs of Synthesised TiO_2 and $CaCO_3$-TiO_2 at different Magnifications Showing Flower-Like Clusters

SEM-EDS of $CaCO_3$-doped TiO_2

The SEM image of the $CaCO_3$-TiO_2 nanocomposite (Fig.-3b) reveals a slightly agglomerated morphology with roughly spherical particles forming clustered structures. Compared with the undoped TiO_2, the doped sample exhibits a relatively rough, porous surface texture. According to the scale bar, the particle size ranged from 80–150 nm for individual particles and up to 300–400 nm for agglomerated clusters. The EDS spectrum (Fig.-4(c)) confirms the existence of Ti, O, Ca, and C, indicating $CaCO_3$ within the TiO_2 matrix incorporation. The absence of additional impurity peaks suggests good elemental purity of the composite. The elemental mapping results (Fig.-4(d)) demonstrate a homogeneous distribution of Ti, O, Ca, and C across the analysed region, supporting uniform dispersion of $CaCO_3$ within the TiO_2 structure.

Dynamic Light Scattering (DLS)-zeta Analysis

DLS measurements were performed at 25 °C in ethanol as a dispersion medium to determine the particle size distribution. Before measurement, all samples were sonicated for 5 min to minimise agglomeration.

Synthesized TiO_2

DLS and zeta potential analyses of synthesized TiO_2 (Fig.-5(a)) exhibited large hydrodynamic diameters in the range of 12.6-23.8 μm with high PDI values (~0.77), indicating significant agglomeration and

broad size distribution in ethanol. Such behaviour is typical for metal oxide NPs due to high surface energy and limited electrostatic stabilization in non-aqueous media.[18] The measured zeta potential values were between -10 and -12 mV, suggesting low dispersion stability and a tendency toward clustering. The large hydrodynamic sizes observed in DLS reflect the suspension behaviour of the NPs in ethanol rather than the primary crystallite size determined by XRD. The observed agglomeration can therefore be attributed to interparticle interactions under the given dispersion conditions.

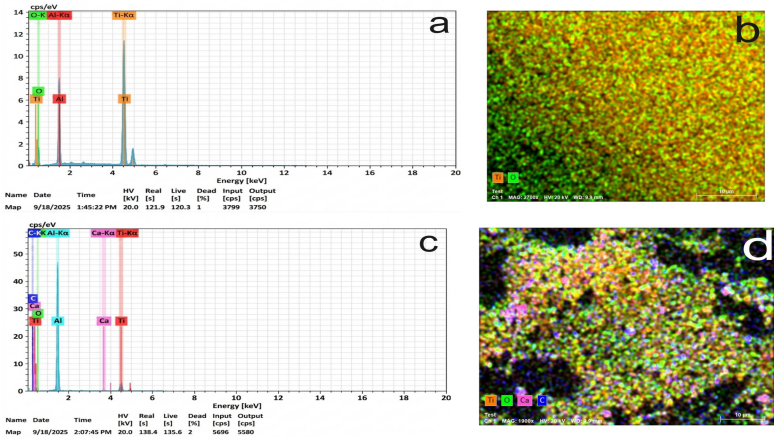

Fig.-4: EDS Analysis of Synthesized TiO_2 and $CaCO_3$–TiO_2 Nanocomposite: (a) EDS Spectrum of Synthesized TiO_2 Showing the Presence of Ti and O, Confirming Phase Purity; (b) EDS Elemental Mapping of TiO_2 Illustrating Uniform Distribution of Ti and O; (c) EDS Spectrum of $CaCO_3$–TiO_2 Confirming the Appearance of Ti, O, Ca, and C, Indicating Incorporation of $CaCO_3$; (d) EDS Elemental Mapping of $CaCO_3$–TiO_2 Showing Homogeneous Distribution of all Constituent Elements

$CaCO_3$-doped TiO_2

The CaCO3-doped TiO_2 composite was similarly analysed by DLS analysis (Fig.-5(b)). The measured hydrodynamic diameters were approximately 383.3, 489.6, and 536.3 nm, indicating the presence of particle aggregates in the dispersion. The corresponding PDI values (0.313-0.472) suggest a moderately polydisperse system with improved distribution compared to the undoped TiO_2 sample. Zeta potential values from +29.6 to +31.1 mV indicate moderate to good electrostatic stability of the nanocomposite dispersion. The stability of the doped sample slightly improves compared to pure TiO_2, which may be cause of the presence of $CaCO_3$ on the TiO_2 surface, which can influence interparticle interactions and dispersion behaviour. Overall, the DLS results suggest that $CaCO_3$ modification contributes to improved stability of dispersion while maintaining a nanoscale aggregated structure. A summary of DLS parameters for both synthesised and doped nanoparticle samples is in Table-1.

Table-1: Summary of DLS-Zeta Potential Parameters of Synthesized TiO_2 and CaCO–doped TiO_2 Nanoparticles

Parameter	Pure TiO_2	$CaCO_3$–TiO_2
DLS size	12.6-23.8 µm	226-251 nm
PDI	0.77	0.31-0.47
Zeta potential (mV)	-10 to -12 mV	+29.6 to +31.1 mV

UV-Visible Diffuse Reflectance Spectroscopy (UV-DRS)

The optical properties of TiO_2, $CaCO_3$-TiO_2 nanomaterial additives (Fig.-6) were analysed using UV-DRS. The synthesized TiO_2 (Fig.-6(a)) exhibited an absorption edge at approximately 390 nm, corresponding to a calculated band gap energy of 3.15 eV (Fig.-6(b)), which is a characteristic of anatase-phase TiO_2. Following $CaCO_3$ incorporation (Fig.-6(c)), the absorption graph shifted slightly to 382 nm, resulting in an energy gap of ~3.24 eV (Fig.-6(d)). The resulting band gap energies were obtained using the relation $E = 1240/\lambda$[19], and further supported by Kubelka-Munk transformed plots[20] derived from the reflectance data. The primary band gap values are consistent with anatase-phase TiO_2, in agreement with XRD observations. The absence of impurity peaks and the preservation of the anatase structure even after $CaCO_3$ incorporation demonstrate that the synthesis route effectively stabilised the crystalline phase.

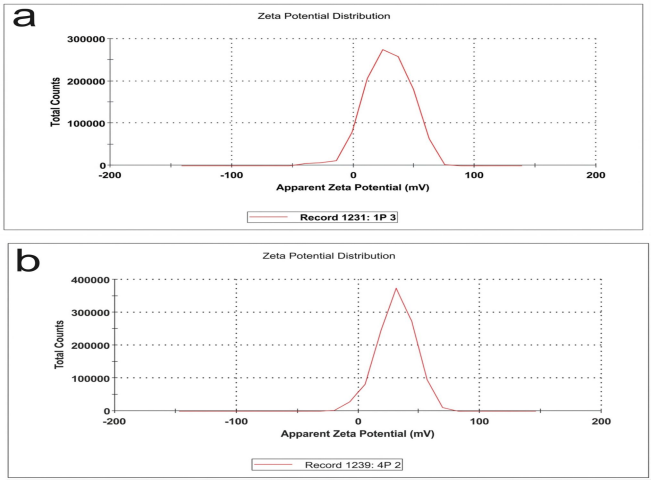

Fig.-5: DLS Analysis of Synthesized TiO_2 and $CaCO_3$–TiO_2 Nanocomposites: (a) Particle Size Distribution of Synthesized TiO_2 Showing Larger Hydrodynamic Size and Lower Stability; (b) Zeta Potential of $CaCO_3$–TiO_2 Indicating Improved Dispersion Behaviour and Enhanced Electrostatic Stability

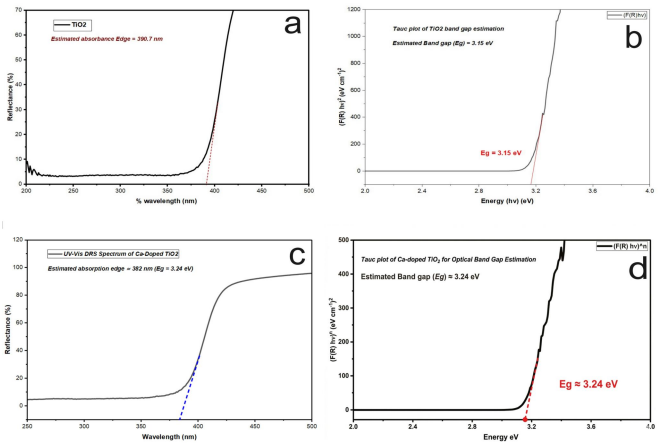

Fig.-6: UV–Visible Diffuse Reflectance Spectra (UV–DRS) and Corresponding Band Gap Analysis of (a, b) Synthesized TiO_2 and (c, d) $CaCO_3$-doped TiO_2 Nanoparticles. (a, c) Diffuse Reflectance Spectra Showing Absorption Edge Behaviour, and (b, d) Kubelka–Munk Plots Used for Band Gap Estimation

FTIR Spectroscopic Analysis

Synthesized TiO_2

The FTIR spectrum of synthesised TiO_2 (Fig.-7(a)) exhibits a broad absorption band at 3351 cm^{-1}, corresponding to O-H stretching vibrations and adsorbed moisture. The band observed at 1626 cm^{-1} is assigned to H-O-H bending vibrations of physically adsorbed H_2O molecules, indicating the hydrophilic nature of the NPs[1]. A band at 1228 cm^{-1} may be associated with Ti-O-C vibrations or residual species from the precursor or synthesis medium. The characteristic absorption peak at 535 cm^{-1} shows the Ti-O lattice, suggesting the formation of TiO_2 NPs.

$CaCO_3$-doped TiO_2

The FTIR spectrum of $CaCO_3$-doped TiO_2 nanocomposite (Fig.-7(b)) shows distinct vibrations with various peaks at 3351, 2361, 1798, 1613, 1425, 875, and 544 cm^{-1}, respectively. The broad, centred peak at 3351 cm^{-1} represents the O-H stretch; 1613 cm-1 is considered the H-O-H bending mode of adsorbed water. The prominent peak absorptions at 1425 cm^{-1} and 875 cm^{-1} are characteristic of CO_3^{2-} vibrations (asymmetric stretching and out-of-plane bending, respectively), confirming the carbonate species ($CaCO_3$) were present in the doped sample. The lower band at 544 cm^{-1} corresponds to Ti–O–Ti lattice vibrations, indicating that the TiO_2 framework is retained after doping. These results confirm the successful incorporation of $CaCO_3$ on the TiO_2 lattice.

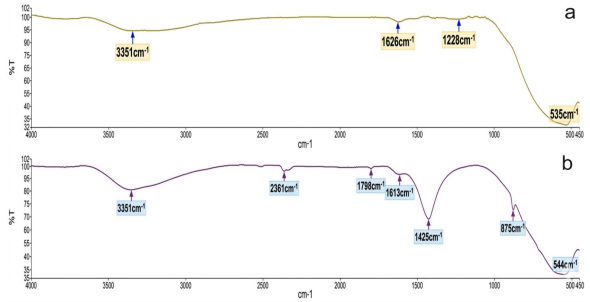

Fig.-7: FTIR Spectra of (a) Synthesized TiO_2 and (b) $CaCO_3$-doped TiO_2 Nanoparticles, Illustrating O–H Stretching, H–O–H Bending, Ti–O–Ti Lattice Vibrations, and Characteristic Carbonate (CO_3^{2-}) Peaks Confirming $CaCO_3$ Incorporation

CONCLUSION

$CaCO_3$-modified TiO_2 NPs were successfully synthesised via a combined sol-gel and wet-impregnation approach. The formation of anatase-phase TiO_2 with successful incorporation of $CaCO_3$, confirmed by the structural and spectroscopic analysis, is evidenced by characteristic diffraction peaks, functional vibration, and optical absorption behaviour. Morphology revealed agglomerated nanostructures with rough and porous surface features, while elemental analysis confirmed uniform distribution of Ti, O, Ca, and C within the composite. DLS and zeta potential parameters show improved dispersion stability for the $CaCO_3$-TiO_2 system compared to the undoped TiO_2 nanostructure. These reports demonstrate that the $CaCO_3$ modification influences the structural, surface, and dispersion characteristics of TiO_2 without altering its fundamental crystalline phase. Such properties are commonly combined with nanomaterials explored for multifunctional applications, including photocatalysis and lubricant additive systems.[14,15] Synthesised TiO_2 was expected to predominantly exhibit the anatase phase[1], which is favourable for lubrication-related surface modification, coating applications and further doping process. However, the actual performance in these applications was not evaluated in the present study and requires further investigation. Overall, this study provides a foundation for future studies on $CaCO_3$-TiO_2 nanocomposites, particularly in the development of environmentally compatible nanomaterials for advanced industrial applications.

ACKNOWLEDGMENTS

The Authors acknowledge the financial support provided by the Ministry of Ports, Shipping and Waterways (MoPSW), Government of India, under the Green Shipping Initiative and the Indian Maritime University for providing institutional support and research facilities.

CONFLICT OF INTERESTS

The authors declare that there is no conflict of interest.

AUTHOR CONTRIBUTIONS

The present work is related to *SDG-9: Innovation and Infrastructure*. All the authors contributed significantly to this manuscript, participated in reviewing/editing and approved the final draft for publication. The research profile of the authors can be verified from their ORCID ids, given below:

Deekshitha Muppidi http://orchid.org/0009-0003-6255-5722
YVV Satyanarayana Murthy http://orchid.org/0000-0003-2790-7297
Jayagopal Narayanan http://orchid.org/0000-0002-6769-2174
Sandeep Kumar http://orchid.org/0009-0005-7237-185X

Cite this article as: M. Deekshitha *et al.*, *Rasayan J. Chem.*, 19(2), 1209-1216(2026), https://doi.org/10.31788/RJC.2026.1929653.

REFERENCES

1. X. Chen and S.S. Mao, *Chemical Reviews*, **107**, 2891(2007), https://doi.org/10.1021/cr0500535
2. K. Hashimoto, H. Irie and A. Fujishima, *Japanese Journal of Applied Physics*, **44**, 8269(2005), https://doi.org/10.1143/JJAP.44.8269
3. Fujishima, T.N. Rao and D.A. Tryk, *Journal of Photochemistry and Photobiology C: Photochemistry Reviews,* **1**, 1(2000), https://doi.org/10.1016/S1389-5567(00)00002-2
4. C. Birleanu, M. Pustan, M. Cioază, A. Molea, F. Popa and G. Contiu, *Scientific Reports*, **12**, 5201(2022), https://doi.org/10.1038/s41598-022-09245-2
5. A.S. Maddaleno, C. Casellas, E. Teixidó, L. Guardia-Escote, M.P. Vinardell and M. Mitjans, *Nanomaterials*, **15**, 951 (2025), https://doi.org/10.3390/nano15120951
6. R. Ghamarpoor, A. Fallah, M. Jamshidi, N. Elmi Fard and S. Salehfekr, *ACS Omega*, **9**, 25457(2024), https://doi.org/10.1021/acsomega.3c08717
7. M. Kuppusamy, S. W. Kim, K. P. Lee, Y. J. Jo, W. J. Kim, *Nanomaterials*, **14**, 136(2024), https://doi.org/10.3390/nano14020136
8. A.C. Pierre and G.M. Pajonk, *Chemical Reviews*, **102**, 4243(2002), https://doi.org/10.1021/cr0101306
9. T. Sugimoto and X. Zhou, *Journal of Colloid and Interface Science*, **252**, 339(2002), https://doi.org/10.1006/jcis.2002.8480
10. K.D. Kim and H.T. Kim, *Colloids and Surfaces A: Physicochemical and Engineering Aspects*, **207**, 263(2002), https://doi.org/10.1016/S0927-7757(02)00140-1
11. R. Asahi, T. Morikawa, T. Ohwaki, K. Aoki and Y. Taga, *Science,* **293**, 269(2001), https://doi.org/10.1126/science. 1061051
12. S. Sun, H. Ding and X. Hou, *Materials,* **11**, 1131 (2018), https://doi.org/10.3390/ma11071131
13. J. Wang, S. Sun and X. Hou, *Materials*, **12**, 3369 (2019), https://doi.org/10.3390/ma12203369
14. F. Ilie and C. Covaliu, *Lubricants*, **4**, 12 (2016), https://doi.org/10.3390/lubricants4020012
15. Shrivastava, S. Kumar, H. Kumar, S. Chauhan, G. Vashishtha and R. Kumar, *Lubricants*, **13**, 229 (2025), https://doi.org/10.3390/lubricants13050229
16. N. A. M. Nasir, W. M. K. Wan Mohamad Ikhmal, M. A. Badruddin and M. G. Mohd Sabri, *Journal of Dispersion Science and Technology*, **45**, 870 (2024), https://doi.org/10.1080/01932691.2023.2186425
17. B. D. Cullity and S. R. Stock, *Elements of X-Ray Diffraction*, 3rd ed., Prentice Hall, New Jersey, pp. 167–171 (2001).
18. S. Bhattacharjee, *Journal of Controlled Release*, **235**, 337(2016), https://doi.org/10.1016/j.jconrel.2016.06.017
19. R. Zallen and M. P. Moret, *Solid State Communications*, **137**, 154(2006), https://doi.org/10.1016/j.ssc.2005.10.024
20. T. Lindgren, J. M. Mwabora, E. Avendano, J. Jonsson, A. Hoel, C. G. Granqvist and S. E. Lindquist, *Journal of Physical Chemistry B,* **107**, 5709(2003), https://doi.org/10.1021/jp027345j
21. M.N.M. Ibrahim, A. Iqbal, C.C. Shen, S.A. Bhawani and F. Adam, *BMC Chemistry*, **13**, 17 (2019), https://doi.org/10.1186/s13065-019-0537-3
22. Y. Xu and G. Zangari, *Coatings*, **11**, 931 (2021), https://doi.org/10.3390/coatings11080931
23. Lee Eng Oi, M.-Y. Choo, H. V. Lee, H. C. Ong, S. B. A. Hamid & Joon Ching Juan, *RSC Advances*, **6**, 108741 (2016), https://doi.org/10.1039/C6RA22894A
24. Phi Hung Dao, T. V. Nguyen, T. A. Nguyen, T. Y. Oanh Doan, T. H. Hoang, T. T. Le & P. Nguyen-Tri, *Materials Chemistry and Physics*, **272**, 124984(2021), https://doi.org/10.1016/j.matchemphys.2021.124984
25. C. Chang, S. Rad, L. Gan, Z. Li, J. Dai & A. Shahab, *Nanotechnology Reviews*, **12**, 20230150(2023), https://doi.org/10.1515/ntrev-2023-0150
26. F. Zuo, Y. Zhu, T. Wu, C. Li, Y. Liu, X. Wu, J. Ma, K. Zhang, H. Ouyang, X. Qiu and J. He, *Pharmaceutics*, **16**, 1214 (2024), https://doi.org/10.3390/pharmaceutics16061214
27. U.Ş. Öztürk and A. Çitak, *Turkish Journal of Chemistry*, **46**, 1345 (2022), https://doi.org/10.55730/1300-0527.3443

[RJC-9653/2025]